ARL-TN-1251 ● Apr 2025

A 3D-Printed C-Band Antenna Array

by Michael Don, Harvey Tsang, Sean Jackson, Kevin Brower, Jonathan Hallameyer, and Macs Brown

NOTICES

Disclaimers

ARL-TN-1251 ● APR 2025

A 3D-Printed C-Band Antenna Array

Michael Don and Harvey Tsang
DEVCOM Army Research Laboratory

Kevin Brower
DEVCOM C5ISR

Sean Jackson
Oak Ridge Associated Universities

Jonathan Hallameyer and Macs Brown
SURVICE Engineering Company

REPORT DOCUMENTATION PAGE

1. REPORT DATE	2. REPORT TYPE	3. DATES COVERED START DATE	END DATE
April 2025	Technical Note	05/20/2024	03/03/2025

4. TITLE AND SUBTITLE
A 3D-Printed C-Band Antenna Array

5a. CONTRACT NUMBER	5b. GRANT NUMBER	5c. PROGRAM ELEMENT NUMBER

5d. PROJECT NUMBER	5e. TASK NUMBER	5f. WORK UNIT NUMBER

6. AUTHOR(S)
Michael Don, Harvey Tsang, Sean Jackson, Kevin Brower, Jonathan Hallameyer, and Macs Brown

7. PERFORMING ORGANIZATION NAME(S) AND ADDRESS(ES)
DEVCOM Army Research Laboratory
ATTN: FCDD-RLA-WE
Aberdeen Proving Ground, MD 21005

8. PERFORMING ORGANIZATION REPORT NUMBER
ARL-TN-1251

9. SPONSORING/MONITORING AGENCY NAME(S) AND ADDRESS(ES)	10. SPONSOR/MONITOR'S ACRONYM(S)	11. SPONSOR/MONITOR'S REPORT NUMBER(S)

12. DISTRIBUTION/AVAILABILITY STATEMENT
DISTRIBUTION STATEMENT A. Approved for public release: distribution unlimited.

13. SUPPLEMENTARY NOTES
ORCIDs: Michael Don, 0000-0002-8021-9066; Harvey Tsang, 0000-0003-3081-9693

14. ABSTRACT
ARL has been researching modeling methods, severe platform-constrained designs, and direction of arrival applications for antenna arrays, as well as materials and methods for 3D printing. This report describes ARL's efforts to combine these research areas by producing a 3D-printed antenna array. First, the design and prototyping of the array is described. Next, the modeling and simulation of a 3D-printed version of the array is presented, and the 3D printing process is detailed. Finally, the test setup and measurement results are given. With this successful manufacturing of a 3D-printed antenna array, ARL is poised to conduct future research developing arrays with more advanced structures and integrated electronics.

15. SUBJECT TERMS
antenna array, 3D printing, antenna measurement, additive manufacturing, direction of arrival, patch antenna, Sciences of Extreme Materials, Weapons Sciences

16. SECURITY CLASSIFICATION OF: a. REPORT	b. ABSTRACT	C. THIS PAGE	17. LIMITATION OF ABSTRACT	18. NUMBER OF PAGES
UNCLASSIFIED	UNCLASSIFIED	UNCLASSIFIED	UU	42

19a. NAME OF RESPONSIBLE PERSON	19b. PHONE NUMBER *(Include area code)*
Harvey Tsang	(301) 394-5734

STANDARD FORM 298 (REV. 5/2020)
Prescribed by ANSI Std. Z39.18

Contents

List of Figures

List of Tables

1. Introduction

Antenna arrays are composed of multiple antenna elements arranged in a specific configuration that are designed to work together to perform advanced signal processing techniques. One key application of antenna arrays is beam steering, where the direction of the antenna's radiation pattern can be adjusted by controlling the phase and amplitude of the signal at each element, improving communication efficiency and reducing interference. Another important application is the determination of the direction of arrival (DOA) of incoming signals, which can be used to locate sources of interference or for network localization. By analyzing the phase differences between array elements, the angle of incoming signals can be accurately estimated (Mailloux 2017).

3D printing, also known as additive manufacturing, is a technology that creates 3D objects by layering materials based on digital models. Unlike traditional manufacturing methods that often involve subtracting material from a larger block, 3D printing builds objects layer by layer, allowing for intricate designs and customization. This process can use a variety of materials, including plastics and metals, making it a versatile technique for numerous applications. 3D printing enables rapid prototyping, reducing the time and cost associated with product development (Shahrubudin et al. 2019).

Antenna arrays produced by 3D printing can have intricate shapes and embedded features that are difficult or impossible to achieve with traditional manufacturing methods. This capability is particularly beneficial for applications requiring custom conformal arrays and highly integrated systems. Additionally, 3D printing enables rapid prototyping and iterative design processes, allowing the quick testing and optimization of antenna arrays. The ability to integrate multiple functions, such as beam steering and enhanced directionality, directly into the printed structures further enhances the performance and versatility of these antenna arrays, making them a promising solution for next-generation communication technologies (Zhang et al. 2016).

The U.S. Army Combat Capabilities Development Command Army Research Laboratory has been researching modeling methods (Zaghloul et al. 2010), severe platform-constrained designs (Katulka et al. 2007), and DOA applications for antenna arrays (Don 2017; Don and Wessel 2018; Don and Arce 2020). DEVCOM Army Research Laboratory also researched additive manufacturing, including development of electronic material processing for radio frequency applications (Hawasli et al. 2018; Lazarus and Tsang 2020). This report describes the manufacture and testing of a 3D-printed C-band antenna array, combining ARL's antenna array expertise with its experience in additive manufacturing. First, the design and prototyping of the array is described. Next, the modeling and simulation (M&S) of a 3D-printed version of the array is presented, and the 3D printing process is detailed. Finally, the test setup and measurement results are given. The 3D-printed antenna array demonstrated similar performance to the prototype array. With this successful manufacturing of a 3D-printed antenna array, ARL is poised to conduct future research developing arrays with more advanced structures and integrated electronics.

2. Prototype

Figure 1 shows the antenna array prototype constructed using five commercial off-the-shelf (COTS) right-hand circularly polarized 5.8-GHz patch antennas mounted on a 1.75- × 3-inch double-sided FR4 circuit board. A minimum of three antennas are required for both azimuth and elevation DOA measurements, with a fourth antenna added to increase measurement diversity and a fifth antenna dedicated to transmission.

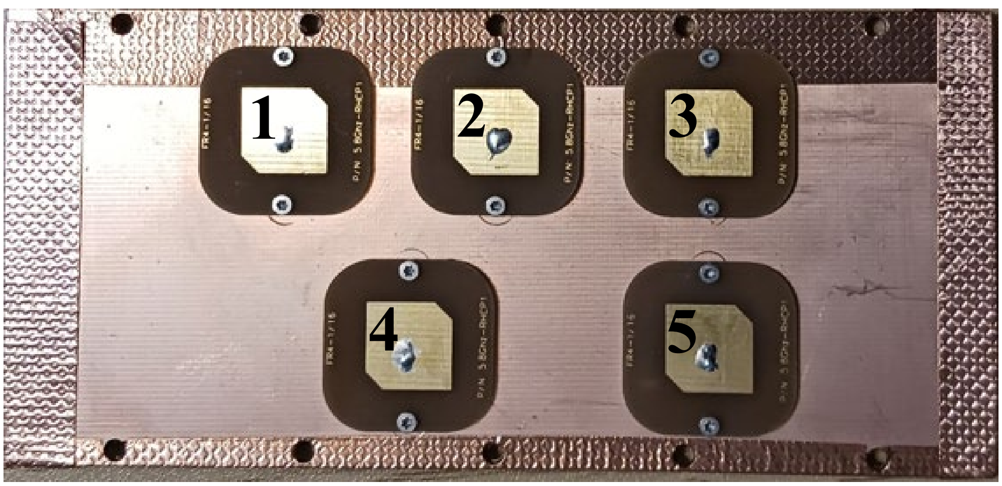

Figure 1. Antenna array prototype.

Figure 2 shows the S11 parameters of the COTS antenna from 5 to 7 GHz. The 5.8-GHz industrial, scientific, and medical (ISM) band is marked by red dashed lines from 5.725 to 5.875 GHz, with the center 5.8-GHz frequency marked by a dashed green line. The performance is adequate, with S11 values ranging from −9.7 to −12.2 within the band. Aside from the minimum S11 value near 5.8 GHz, there is also an even lower valley at −16.8 dB near 6.2 GHz.

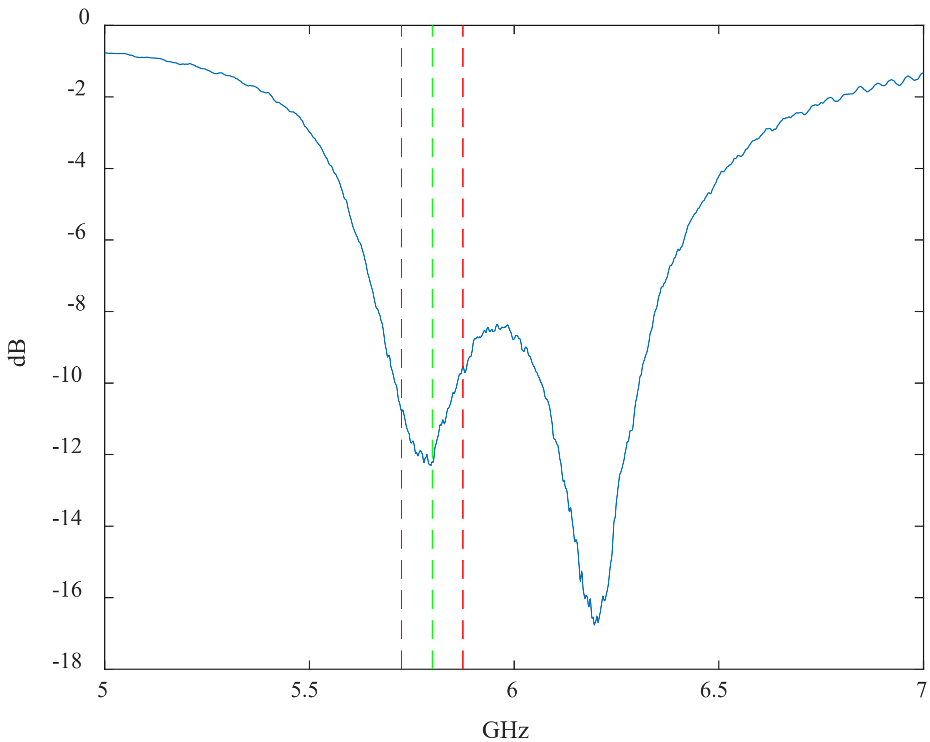

Figure 2. **S11 parameter of the COTS antenna from 5 to 7 GHz. The 5.8-GHz ISM band boundaries are marked by red dashed lines, with the center frequency marked by a dashed green line.**

3. Modeling

M&S was performed to better understand the behavior of 3D-printed antennas, predict the performance of future designs, and predict performance in varying operational environments. CST Suite was the simulation software used to model the microstrip patch antenna array utilizing a finite element method for simulation. An initial digital model was created from the original prototype design, which used traditional manufacturing methods, and the simulation results were compared to the measured results of the fabricated device. Figure 3 presents both (a) the results of the simulated design using original dimensions and (b) the measured results of one of the elements. The primary resonant frequency of the simulation ranges from 5.9 to 6 GHz with a S11 magnitude just below –10 dB. However, at the design frequency of 5.8 GHz, the magnitude ranges from –7 to –8 dB. While the resonant frequency of the measured results of the fabricated sample is shifted higher to around 6.2 GHz with a magnitude of –16.7 dB, the design frequency still performs well at –12 dB.

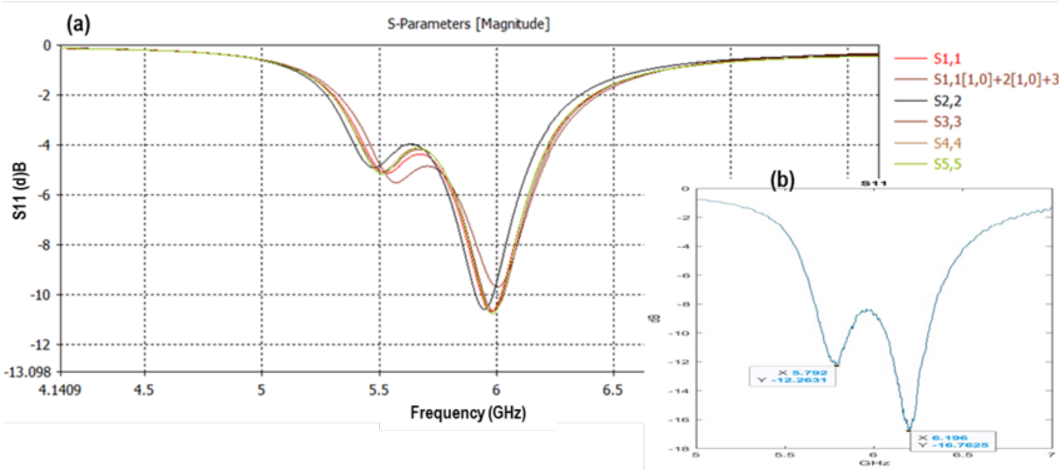

Figure 3. (a) Simulated results of all five original fabricated array elements, and (b) measured results of one element.

The 3D-printed antenna array was also modeled in CST Suite using the measured thickness and width profiles from a Keyence microscope shown in Appendix A, attempting to best represent the fabricated sample. A silver conductive ink with less than bulk silver properties was used in the sample. The formula $\sigma = R_s/t$ was used to calculate the conductivity and was input into CST, where R_s is the surface resistance, σ is the conductivity, and t is the sheet thickness. Using the measured resistivity (0.03 Ω/sq) and the average measured thickness of the elements (0.061 mm), R_s was calculated to be 5.46×10^5 S/m. Surface roughness of 0.001 mm was also input to account for the printed surface.

Other simulation parameters remained the same as those used for Figure 3. Figure 4 shows the simulation results using the updated parameters. Element 1 (*S1,1*) shows the best performance at the design frequency of 5.8 GHz at –10.97 dB with a resonance at 5.72 GHz. As shown in Figure 4, each subsequent element has a shifting resonance to lower frequencies, which likely can be attributed to the increasing widths of the additively fabricated elements. The challenge of accurately capturing the nonprecise fabricated dimensions in the simulated model causes some discrepancies between simulated and measured results and is expected. While the simulated and measured values agree well, the simulation can be improved through more accurate silver ink conductivity measurements, surface roughness characterization, and physical dimension analysis of the elements. Additional simulation results are included in Appendix B.

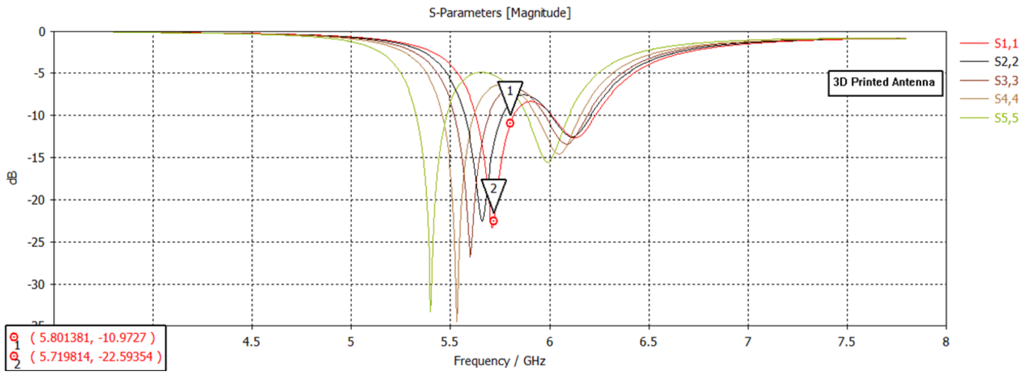

Figure 4. Simulated results of all five 3D-printed antenna elements using the measured thickness and width profiles shown in Appendix B.

4. 3D Printing

Figures 5 and 6 show an example front and back of the printed array, respectively. The FR4 boards were aligned into a ChemCubed ElectroJet system. Silver pads were printed through inkjet print deposition of 18 consecutive layers of particle-free silver ink (C3-AG-1037-2) (ChemCubed) directly onto the FR4 surface of the circuit board. The FR4 surface was plasma treated immediately prior to ink deposition and the entire board was maintained at 70 °C during inkjet printing. After three consecutive layers were deposited, the print tray was extracted for exposure to a secondary heat source. A heat gun emitting heated air at 100 °C was positioned 5 cm above the substrate surface and scanned across the silver pads. This process was repeated 6 times for deposition of 18 total layers. After deposition, average sheet resistance values of 0.03 Ω/sq were measured via four-point probe electrical testing. Profilometry measurements are included in Appendix A.

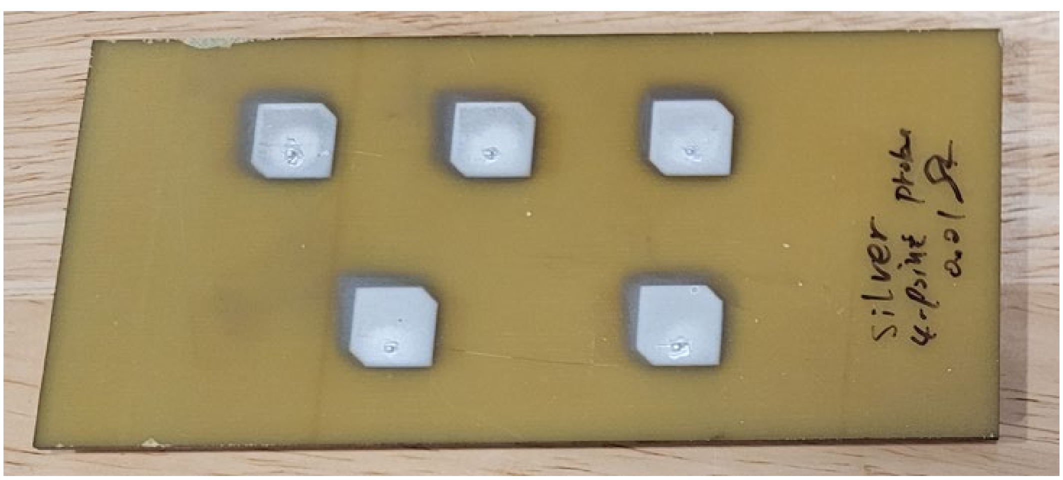

Figure 5. Front of printed array.

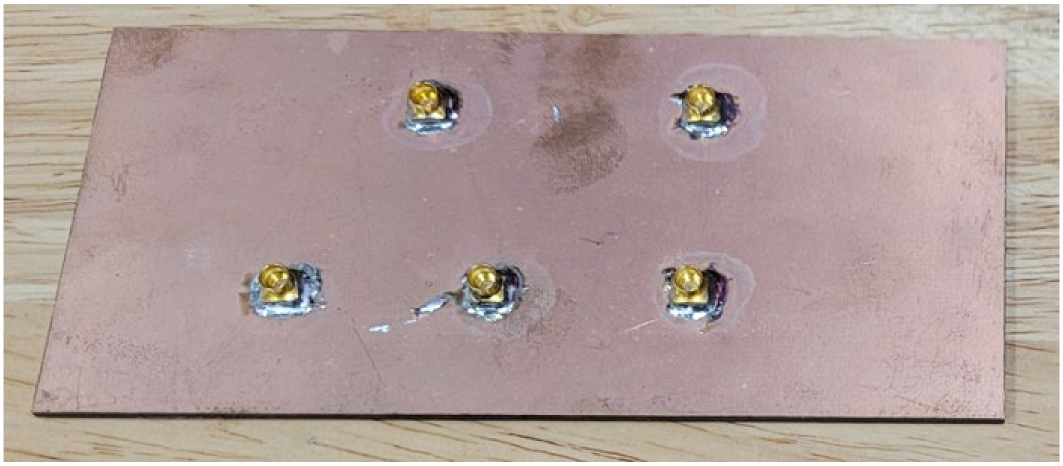

Figure 6. **Back of printed array.**

5. Measurement Setup

Antenna pattern measurements were obtained using a custom antenna measurement system developed by the Guidance Technologies Branch at ARL. Figure 7 shows the system diagram and Figure 8 shows the antenna positioner in the anechoic chamber. The system uses an ETS-Lindgren 2010 multi-axis positioner composed of a 2188 turntable for rotation in azimuth, a light duty tower for rotation in elevation, and a 2090-series multidevice controller that interfaces with the positioner through optical fiber. A network analyzer is connected to the antenna under test (AUT) and transmit antenna to measure gain and phase response. A computer controls the positioner and network analyzer through general purpose interface bus (GPIB) interfaces. National Instruments GPIB-USB-HS adapters were used to provide GPIB control through standard USB ports.

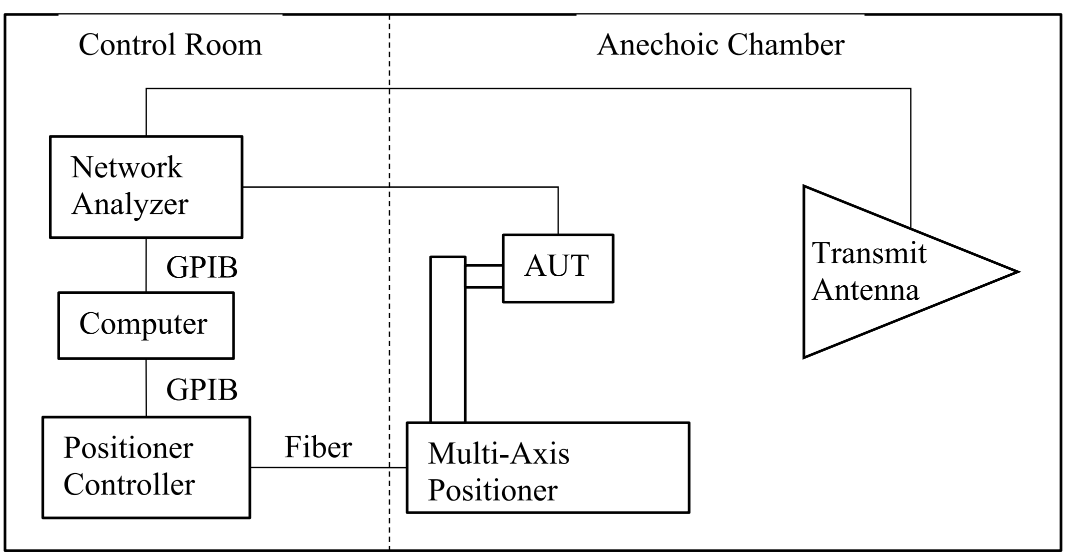

Figure 7. **Antenna pattern measurement system diagram.**

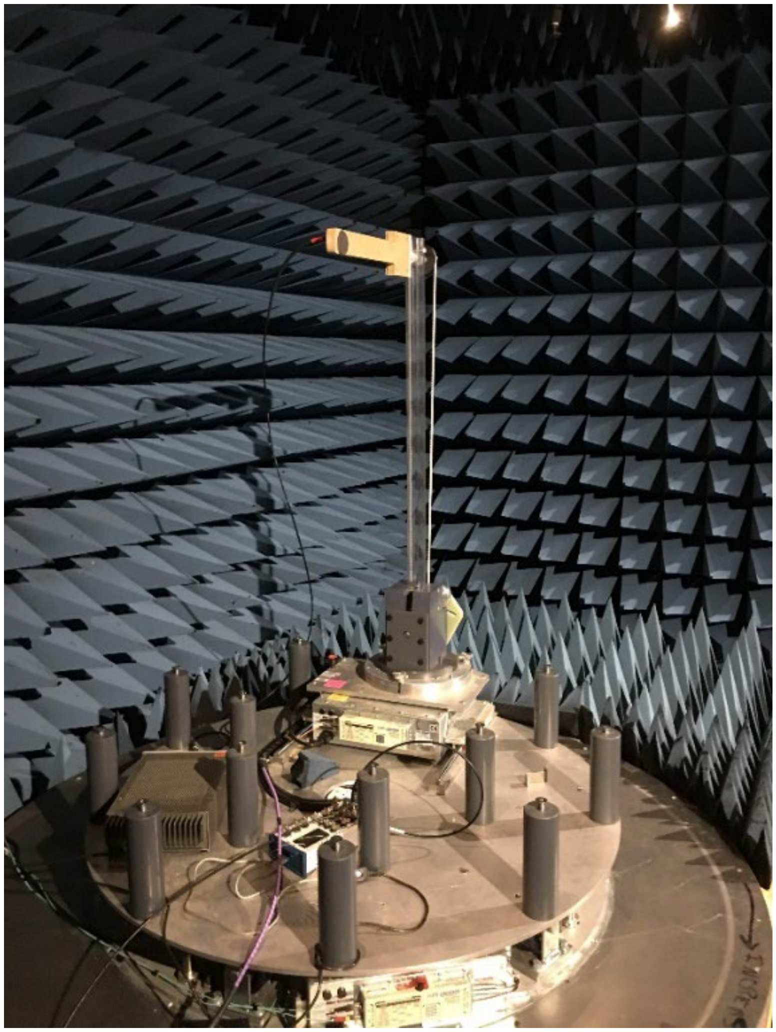

Figure 8. Antenna positioner system in anechoic chamber.

Although ARL had previously developed control software for the antenna measurement system (Don et al. 2021), computer and networking problems prompted the software to be rewritten in Python and run from a standalone computer. The control software is included in Appendix C. Table 1 lists the program's input parameters. The program assumes the azimuth and elevation orientation shown in Figure 9. The positioner itself has an arbitrary, but fixed, real orientation. Therefore, it is necessary to input the positioner's real orientation to calculate the conversion from the assumed orientation to the real orientation. The program starts at the smallest azimuth and elevation values and sweeps in elevation between each increment in azimuth. Each elevation sweep begins at the last elevation position, resulting in a change of direction for each sweep. Data is saved in the order it is acquired; therefore, every other elevation sweep must be reversed when processing the data. If only an azimuth or elevation cut is required, the other field-of-view parameter is set to zero.

Table 1. Antenna measurement input parameters.

Parameter	Description
`az_zero`	Positioner's real orientation considered to be zero degrees azimuth
`az_fov`	Total azimuth sweep angle (degrees)
`az_res`	Azimuth degrees per measurement
`el_zero`	Positioner's real orientation considered to be zero degrees elevation
`el_fov`	Total elevation sweep angle (degrees)
`el_res`	Elevation degrees per measurement
`basename`	Base text used to construct saved file name

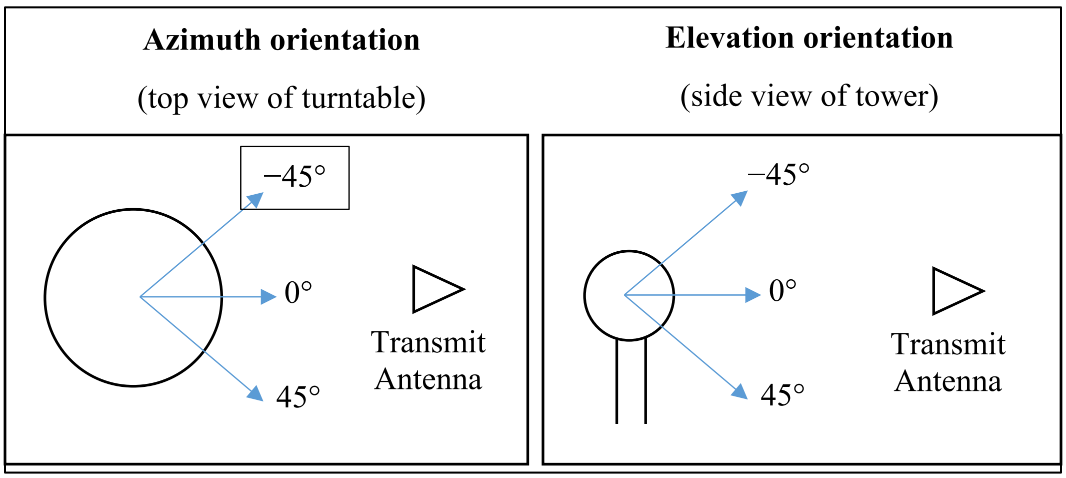

Figure 9. Positioner rotation orientation.

To accurately measure the antenna parameters, the antenna was installed on a representative platform body with the orientation shown in Figure 1. Figures 10 and 11 show a simple two-part shaft coupler designed to attach the body housing to the positioner roll actuator. The coupler was designed to be manufactured by selective laser sintering (SLS) of glass-filled nylon powder. SLS glass-filled nylon was chosen for its strength compared to other additively manufactured materials and because it will not interfere with radio experiments, unlike most metals. Six ribs were added to the coupler to provide better support and rigidity to the cantilever created by the body housing when installed in the coupler.

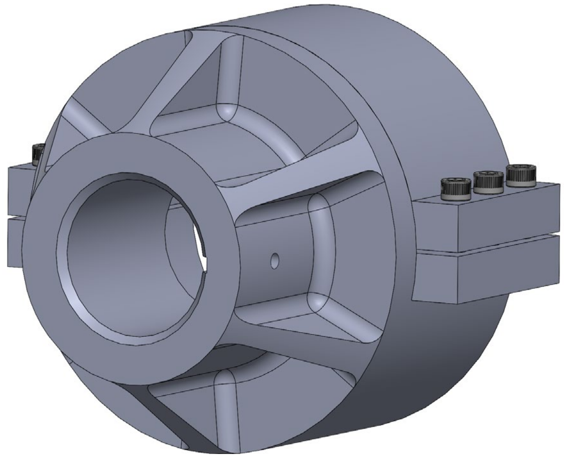

Figure 10. Roll actuator side of the shaft coupler.

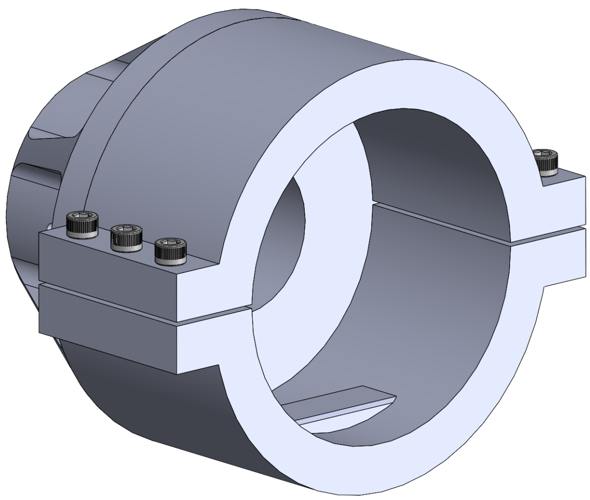

Figure 11. Body housing side of the shaft coupler.

6. Results

The S11 values and antenna patterns of two printed arrays, referred to as "printed 1" and "printed 2," were measured and compared to the prototype array. Figure 12 shows the S11 measurements for the five antenna elements in each printed array, with the 5.8-GHz ISM band indicated as in Figure 2. Figure 13 uses the S11 values of element 2 to compare the printed arrays to the prototype array, which uses COTS antennas. The resonance frequencies of the printed arrays are lower than those of the prototype array. This had favorable results in the case of printed 2, as the second valley in the S11 values coincided with the ISM band. The resonance frequencies for printed 1 were shifted too low, with the peaks occurring below the ISM band. The S11 values for printed 2 were relatively consistent, whereas printed 1 showed more variability. Table 2 summarizes these results, listing frequency and S11 values at the high- and low-frequency valleys for each array, as well as the separation between valleys, the center of the valleys, and the S11 value at 5.8 GHz.

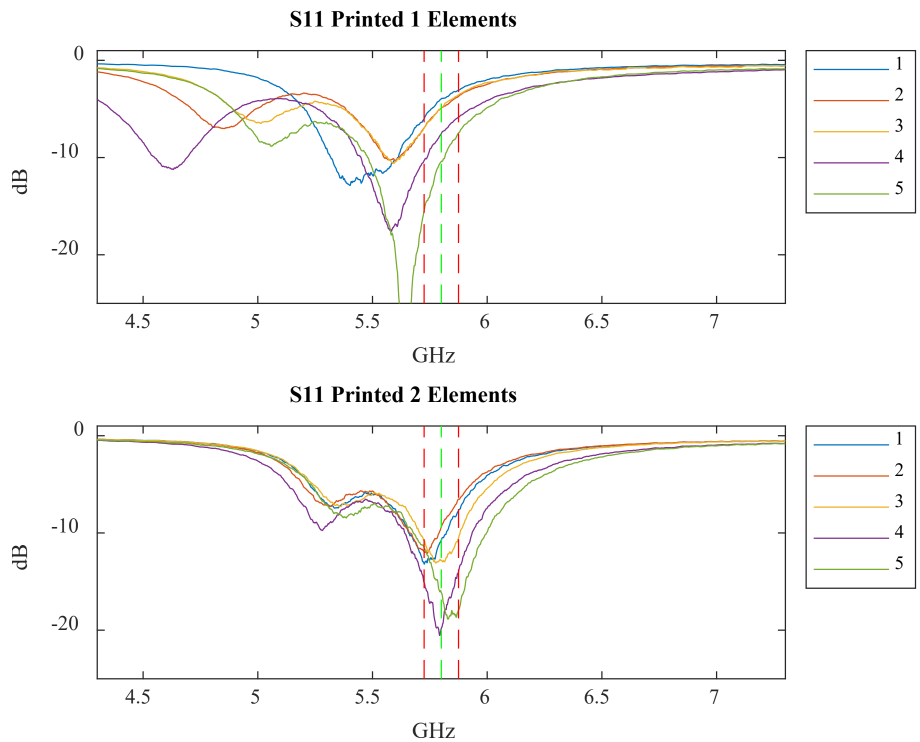

Figure 12. S11 parameter for all five elements of the two printed arrays.

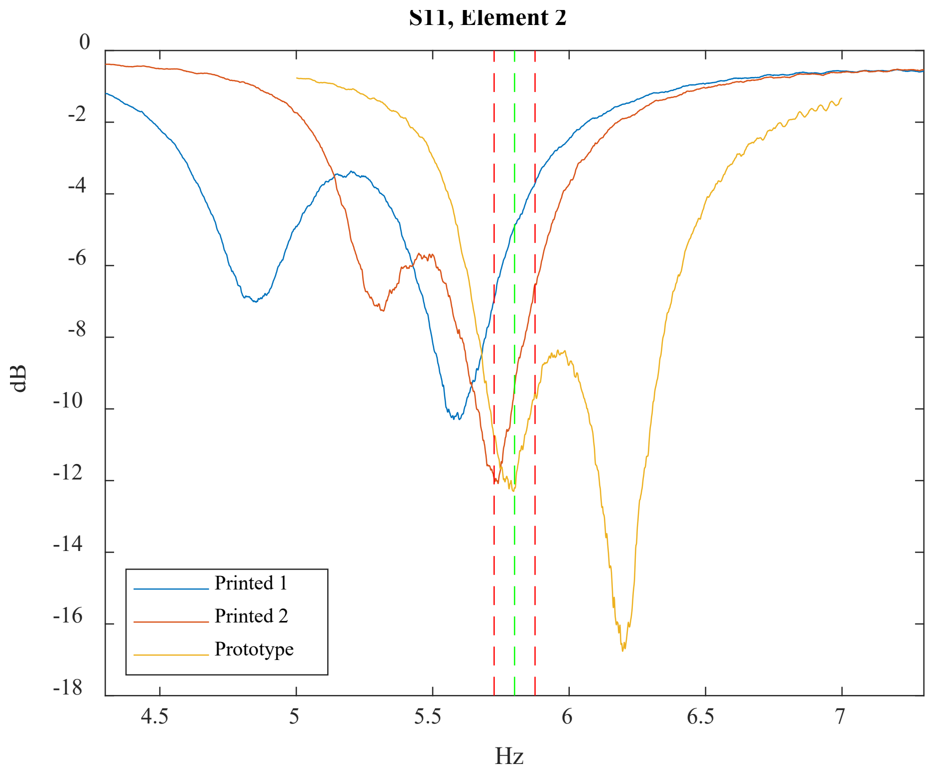

Figure 13. S11 parameter for element 2 of the two printed arrays.

Table 2. Summary of S11 measurement results.

Frequency	Prototype	Printed 1	Printed 2
Low valley frequency (GHz)	5.78	4.84	5.31
High valley frequency (GHz)	6.19	5.58	5.73
Low valley S11	–12.13	–6.99	–7.15
High valley S11	–16.74	–10.21	–12.03
Frequency separation (GHz)	0.41	0.75	0.42
Center frequency (GHz)	5.99	5.21	5.52
S11 at 5.8 GHz	–12.2	–4.9	–9.36

Figure 14 shows an azimuth cut of the antenna patterns at 5.8 GHz for element 2 of the printed and prototype arrays. The measurement setup was not calibrated for absolute measurements but are suitable for a relative comparison. Printed 1 had an average –1.2-dB gain over the prototype array across an 80° span, while printed 2 had a 0.6-dB gain. Similarly, Figure 15 shows the elevation cut of the antenna patterns at 5.8 GHz for element 2 of the printed and prototype arrays. Printed 1 had an average –1.1-dB gain over the prototype array across an 80° span, while printed 2 had a 0.2-dB gain. These results are consistent with the S11 measurements, as the S11 values for printed 2 were lower than those for printed 1. Although the results showed some variability, in general, the printed antenna arrays compared favorably with the prototype array.

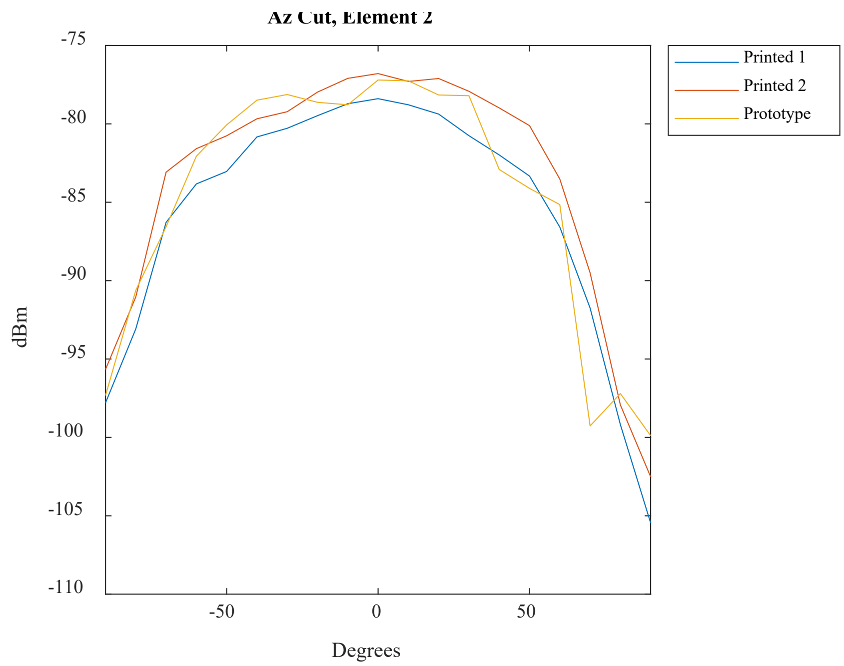

Figure 14. Azimuth cut of the antenna patterns at 5.8 GHz for element 2 of the printed and prototype arrays.

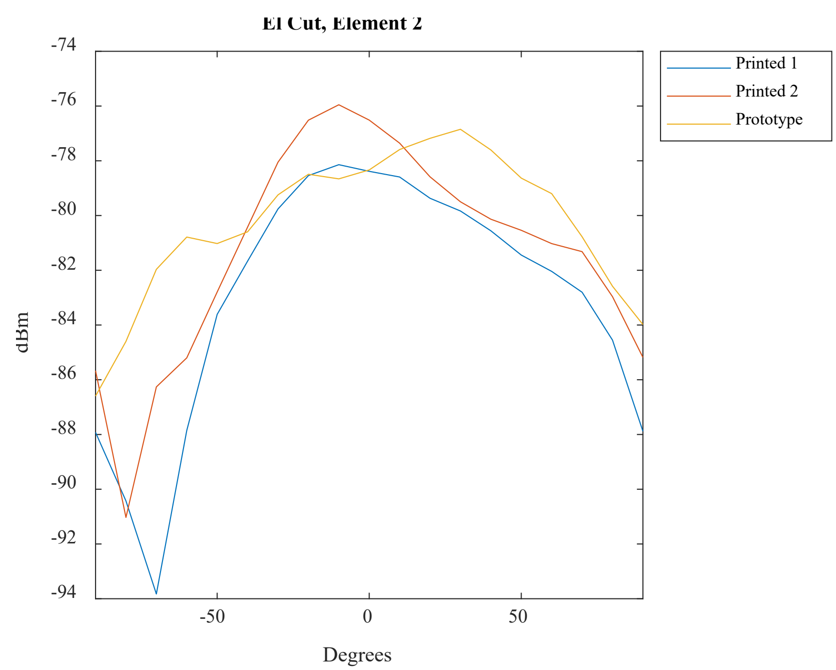

Figure 15. Elevation cut of the antenna patterns at 5.8 GHz for element 2 of the printed and prototype arrays.

Figure 16 shows a comparison of the azimuth cut of the antenna pattern of element 2 of printed 1 at 5.6 and 5.8 GHz. From Table 2, we see that the S11 at 5.6 GHz is about –10 dB, while at 5.8 GHz it is about –5 dB. The average difference in gain between 5.8 and 5.6 GHz over an 80° span is –2.4 dB, demonstrating that the high S11 value at 5.8 GHz for printed 1 degrades the antenna's performance.

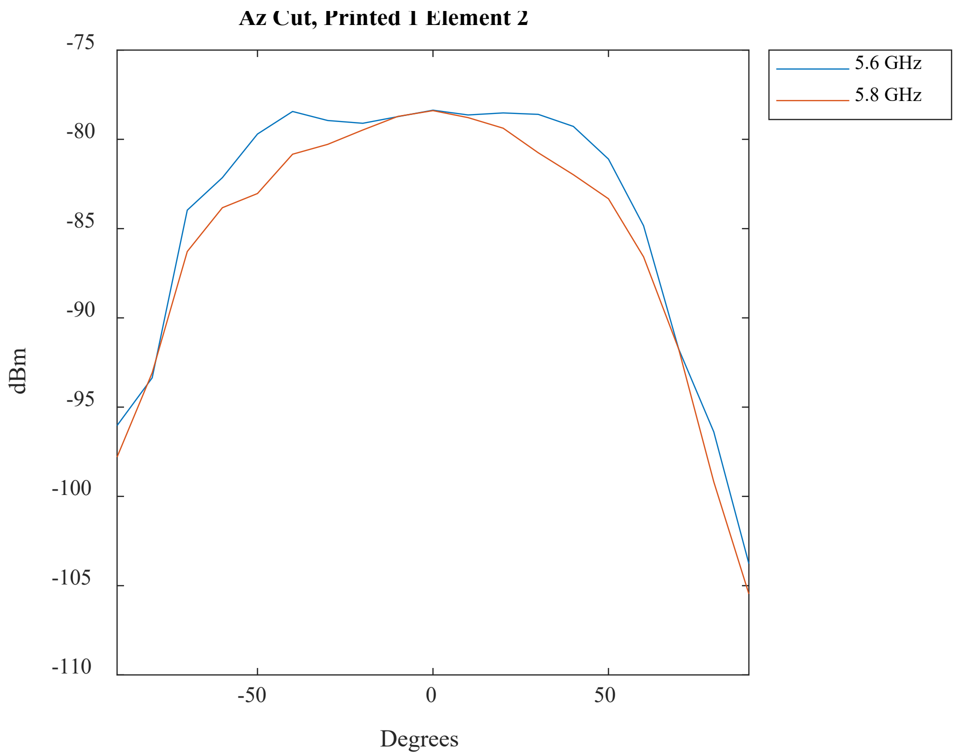

Figure 16. Comparison of the azimuth cut of the antenna pattern of element 2 of printed 1 at 5.6 and 5.8 GHz.

7. Conclusion

This report describes the manufacture and testing of a 3D-printed C-band antenna array. First, the design and prototyping of the array was described. Next, the M&S of a 3D-printed version of the array was presented, and the 3D-printing process was detailed. Finally, the test setup and measurement results were given. In general, the 3D-printed antenna array demonstrated similar performance to the prototype array. There was some variability in the printing process that led to variability in the measured results. Future research will focus on centering the antenna's main resonance frequencies within the ISM band and producing more consistent results. With this successful production of a 3D-printed antenna array, ARL is positioned to research more advanced arrays structures and integrated electronics.

8. References

Don M, Arce G. Antenna pattern measurement with compressive phase retrieval. 2020 IEEE Radio and Wireless Symposium (RWS); 2020 Jan 26. IEEE; c2020. p. 38–38.

Don M, Wessel D. Software-defined radio angle of arrival measurement of modulated signals. Army Research Laboratory (US); 2018 Dec. Report No.: ARL-TR-8601.

Don ML. The feasibility of radio direction finding for swarm localization. Army Research Laboratory (US); 2017. Report No.: ARL-TR-8114.

Don ML, Zajicek JM, Hall RA. A data acquisition system for antenna array gain characterization. DEVCOM Army Research Laboratory (US); 2021. Report No.: ARL-TN-1058.

Hawasli S, Tsang H, Lazarus N, Smith G, Forsythe E. Improving conductivity of 3D printed conductive pastes for RF & high performance electronics. 2018 IEEE MTT-S International Microwave Workshop Series on Advanced Materials and Processes for RF and THz Applications (IMWS-AMP); 2018 July 16–18. IEEE; c2018. p. 1–3.

Katulka G et al. Low-cost rapid-response embedded antenna design for US Army 60MM mortars. International Foundation for Telemetering; 2007.

Lazarus N, Tsang HH. 3-D printing structural electronics with conductive filaments. IEEE Trans Compon Packag Manuf Technol. 2020;10(12): 1965–1972.

Mailloux RJ. Phased array antenna handbook. Artech House; 2017 Nov 30.

Shahrubudin N, Lee TC, Ramlan RJ. An overview on 3D printing technology: technological, materials, and applications. Procedia Manuf. 2019;35:1286–1296.

Zaghloul AI, Weiss SJ, Coburn WK. Antenna developments for military applications. Appl Comput Electromagn Soc J. 2010;25(1):41–53.

Zhang B et al. Metallic 3-D printed antennas for millimeter- and submillimeter wave applications. IEEE Trans Terahertz Sci Technol. 2016;6(4):592–600.

Appendix A. Array Profilometry Measurements

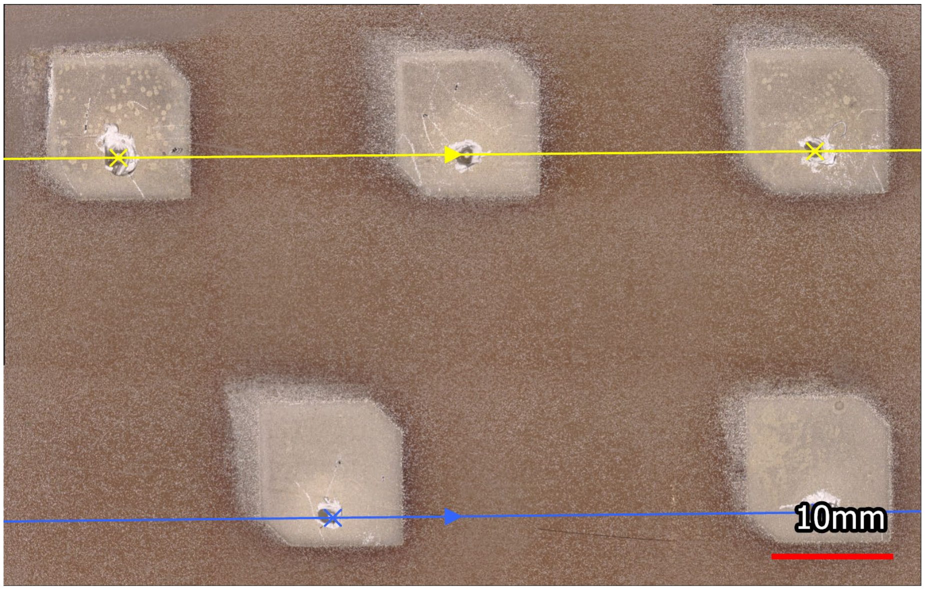

Figure A-1. Optical image of printed array 1 with profilometry lines shown.

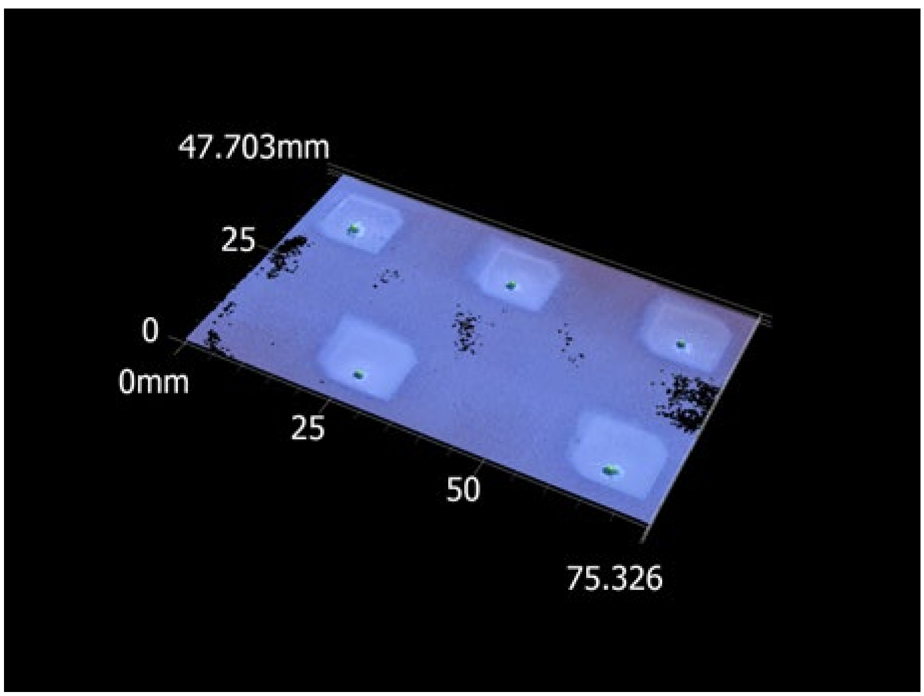

Figure A-2. 3D image of printed array 1.

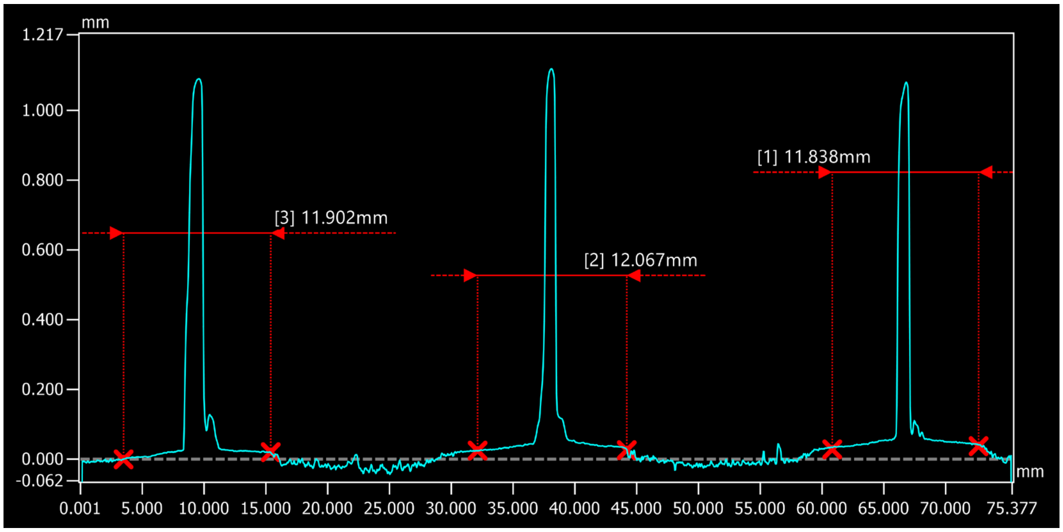

Figure A-3. Profile graph of the yellow line in Figure A-1.

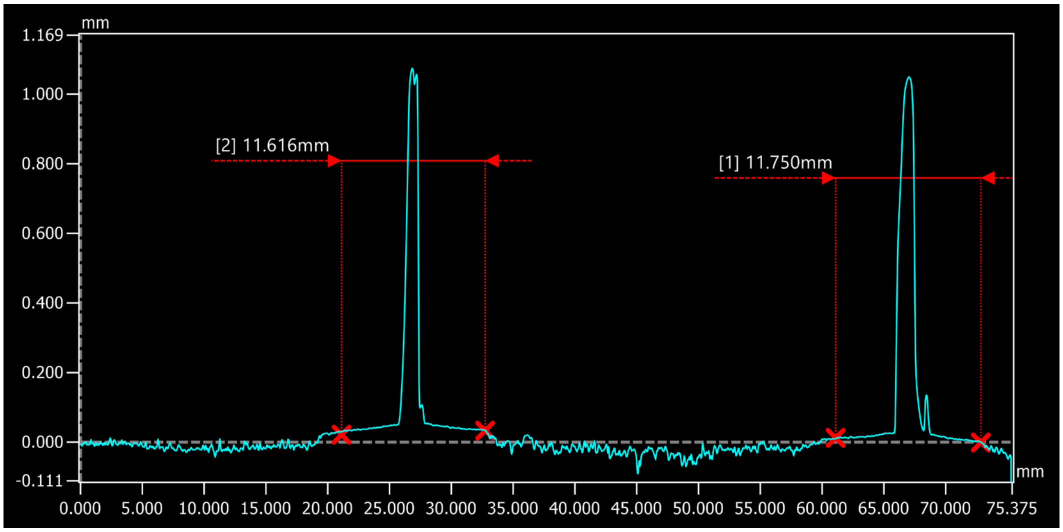

Figure A-4. Profile graph of the blue line in Figure A-1.

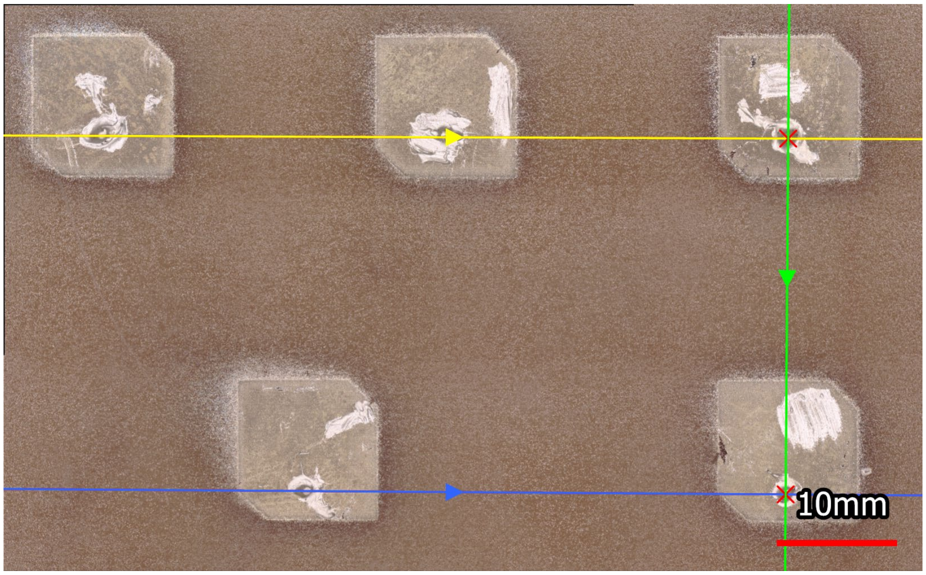

Figure A-5. Optical image of printed array 2 with profilometry lines shown.

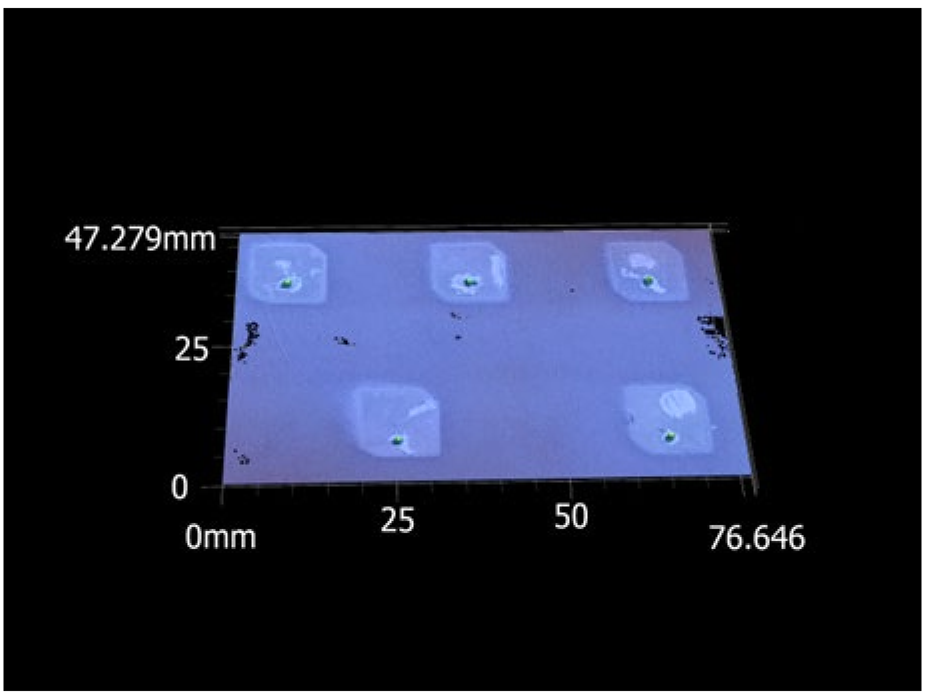

Figure A-6. 3D image of printed array 2.

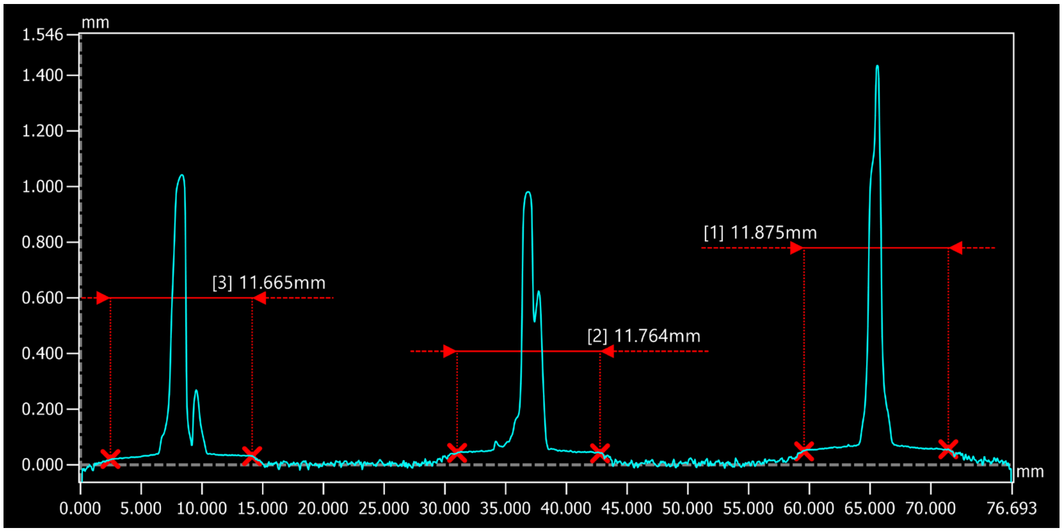

Figure A-7. Profile graph of the yellow line in Figure A-5.

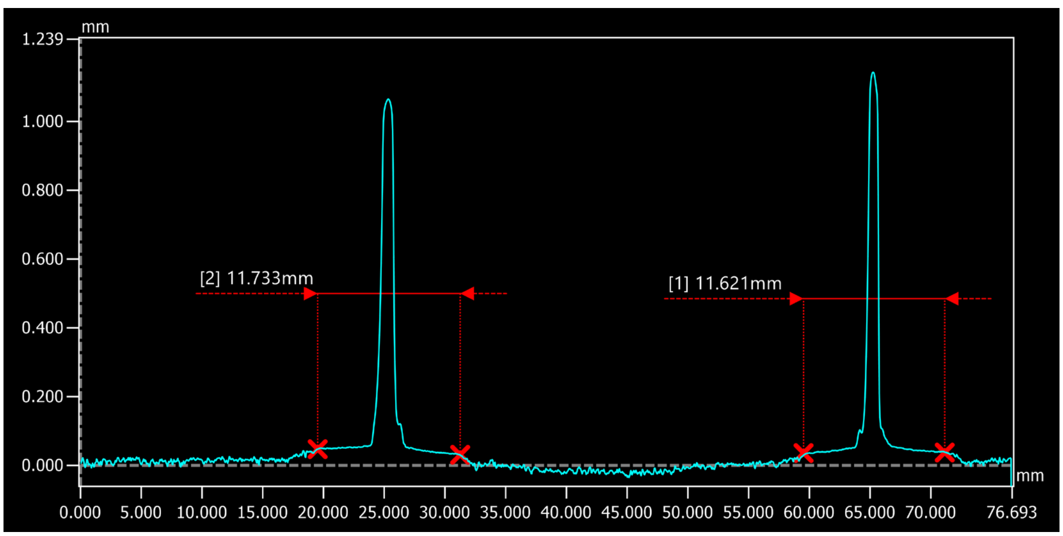

Figure A-8. Profile graph of the blue line in Figure A-5.

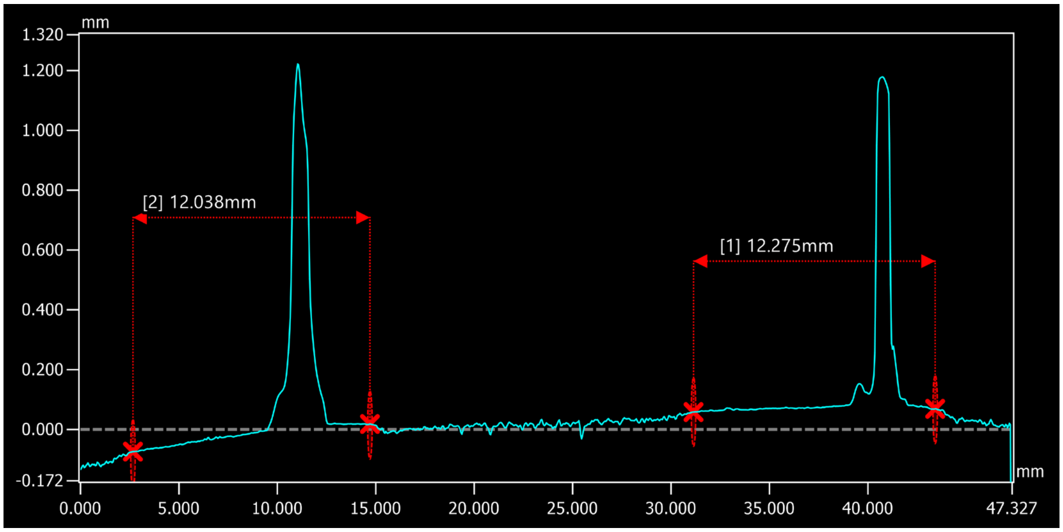

Figure A-9. Profile graph of the green line in Figure A-5.

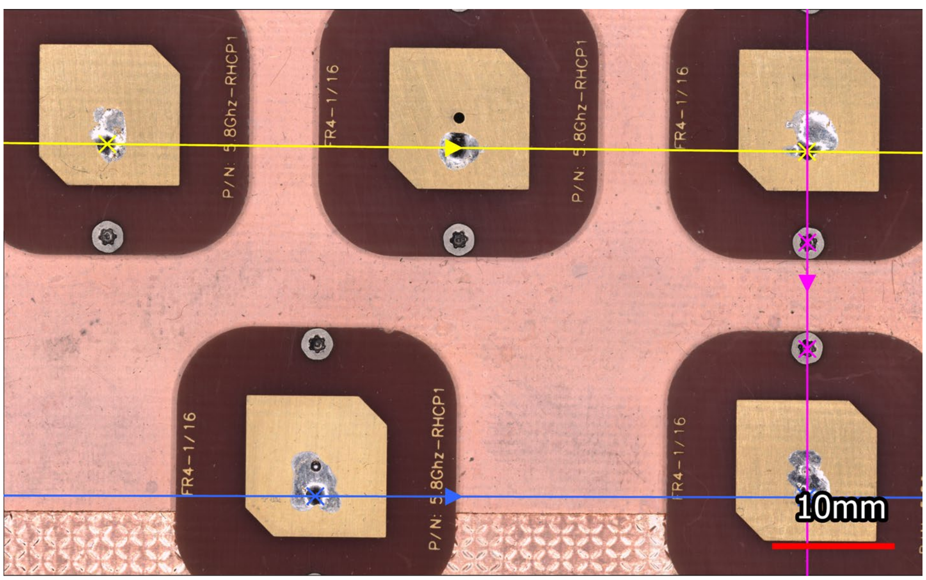

Figure A-10. Optical image of the prototype array with profilometry lines shown.

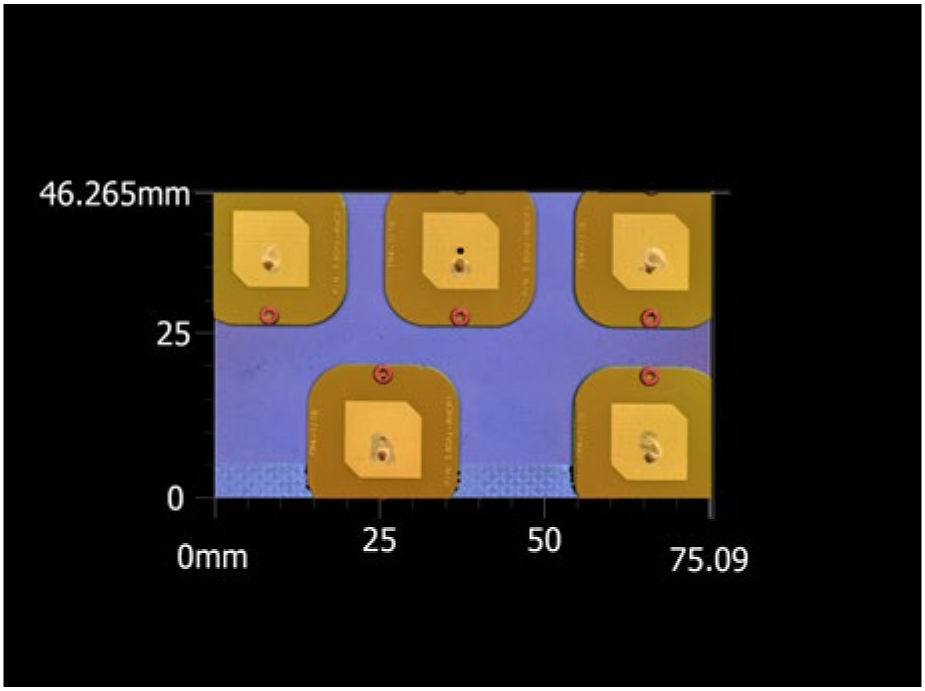

Figure A-11. 3D image of the prototype array.

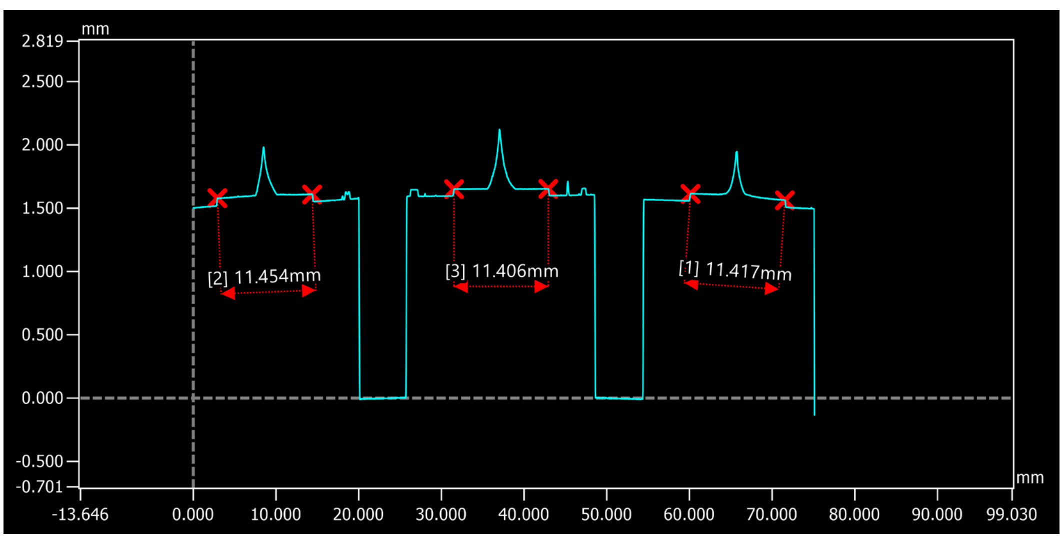

Figure A-12. Profile graph of the yellow line in Figure A-10.

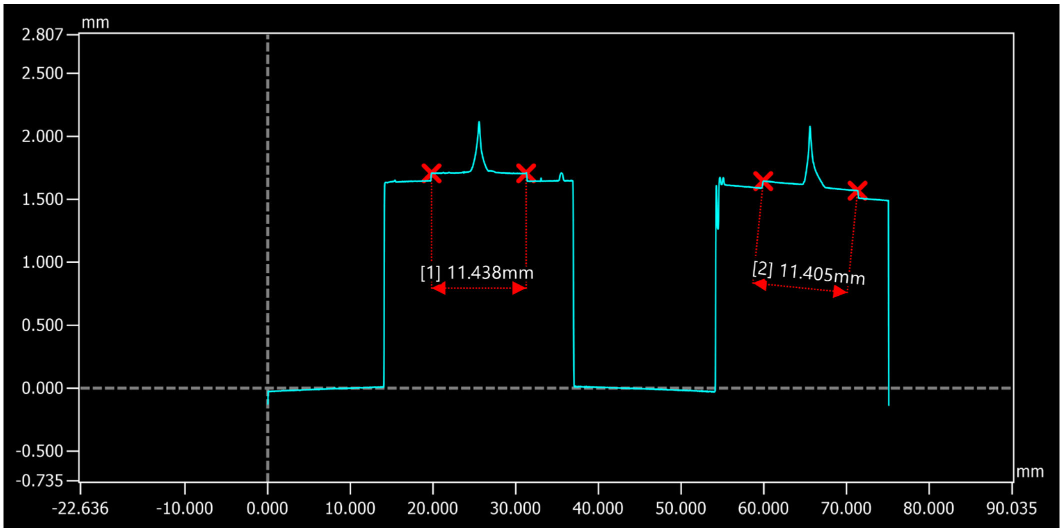

Figure A-13. Profile graph of the blue line in Figure A-10.

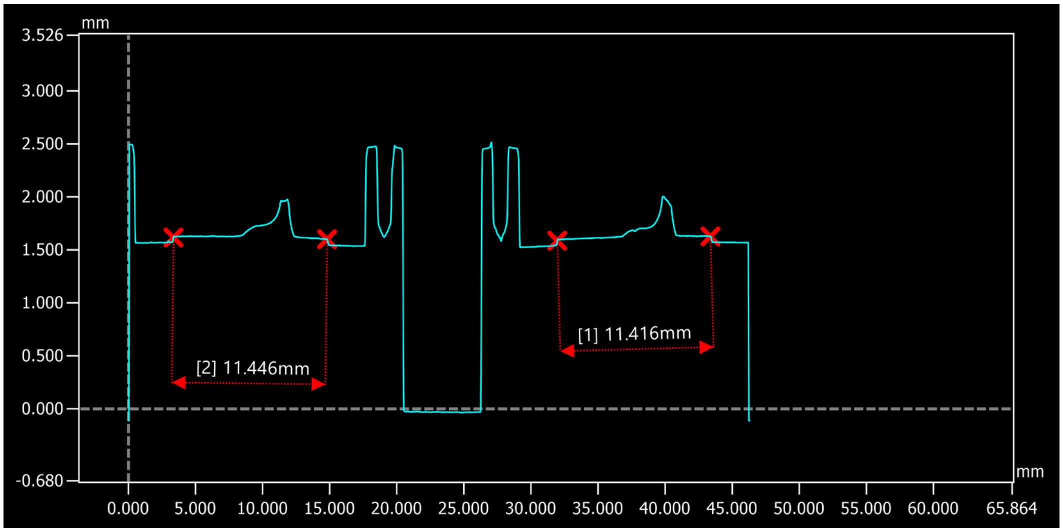

Figure A-14. Profile graph of the magenta line in Figure A-10.

Appendix B. 3D-Printed Array Simulation Results

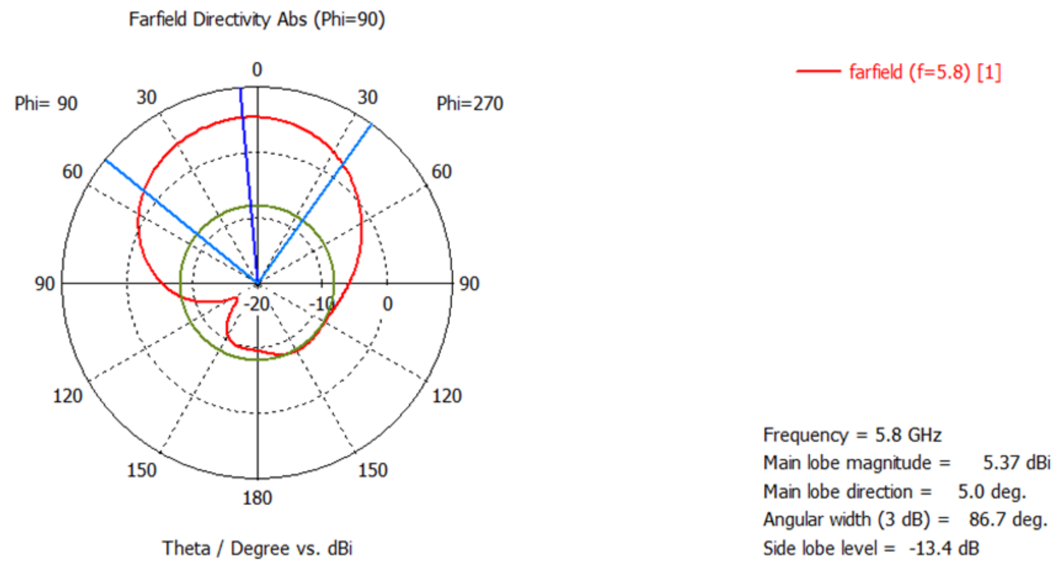

Figure B-1. Simulated directivity of 3D-printed antenna: element 1.

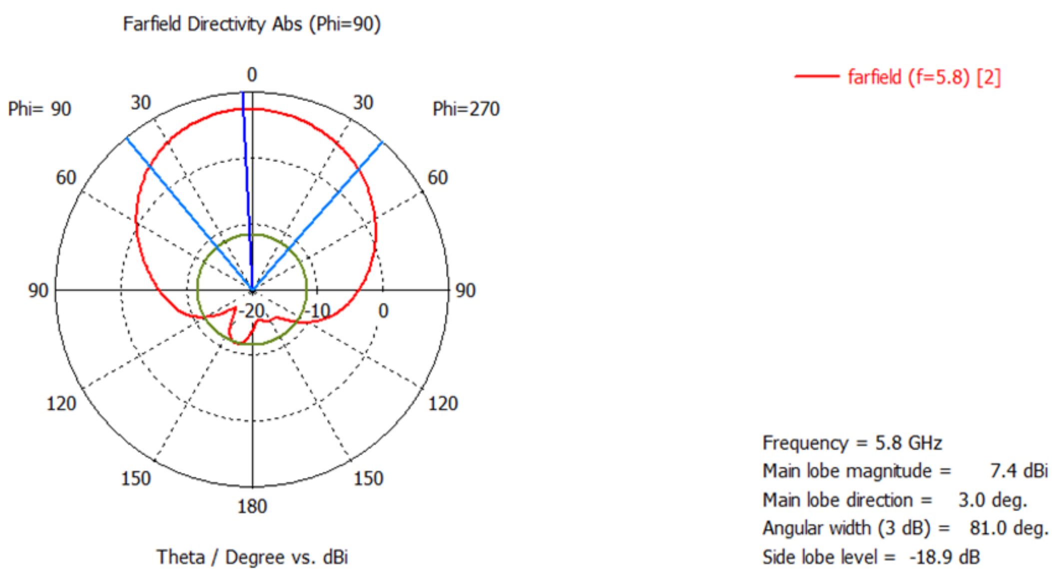

Figure B-2. Simulated directivity of 3D-printed antenna: element 2.

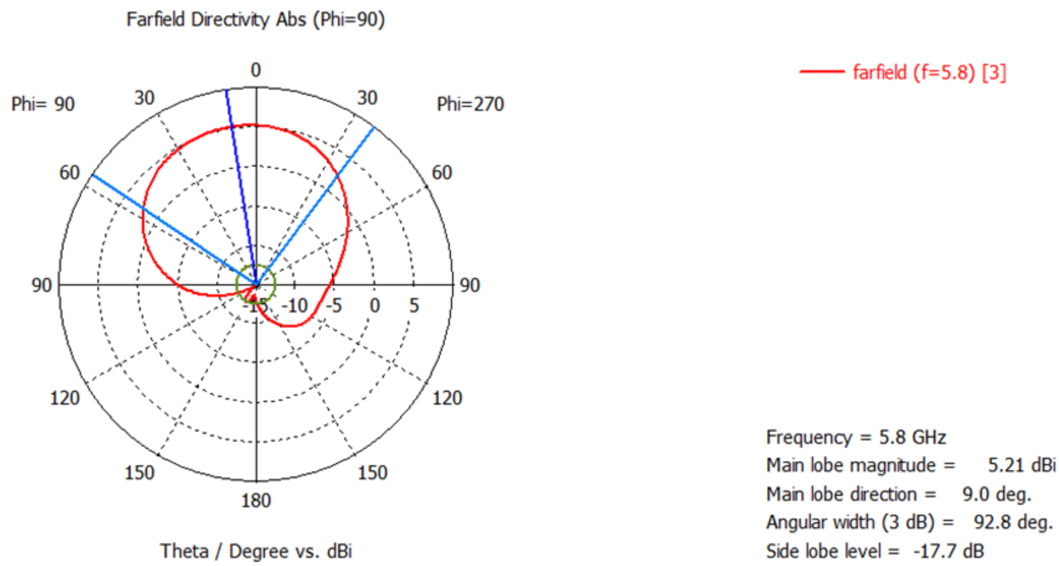

Figure B-3. Simulated directivity of 3D-printed antenna: element 3.

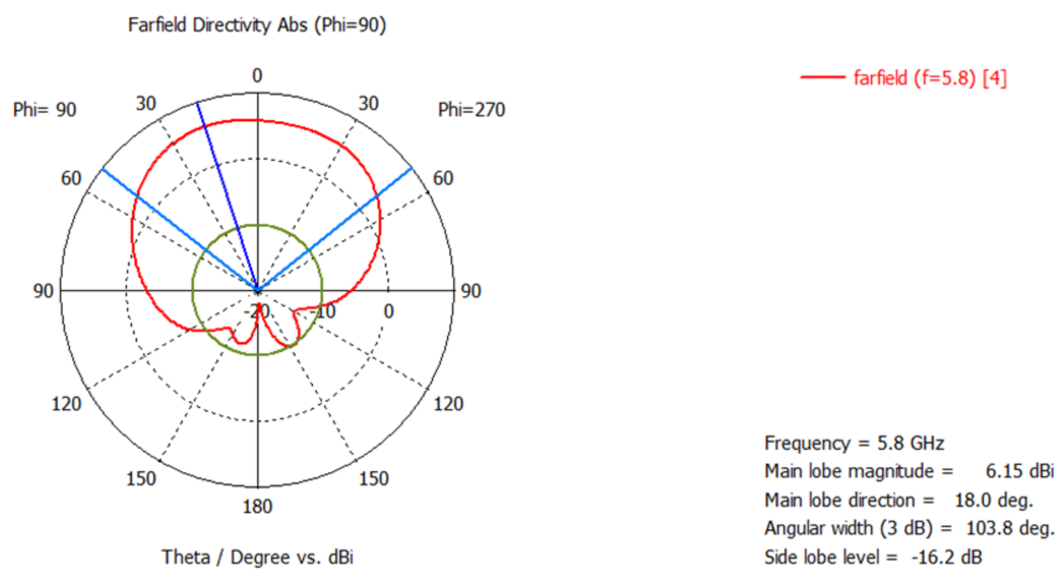

Figure B-4. Simulated directivity of 3D-printed antenna: element 4.

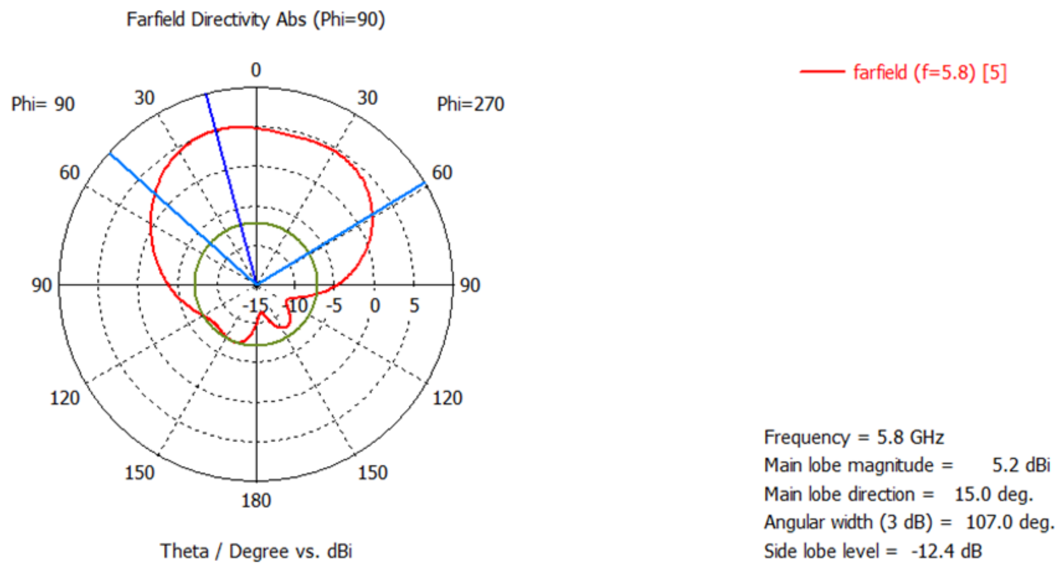

Figure B-5. Simulated directivity of 3D-printed antenna: element 5.

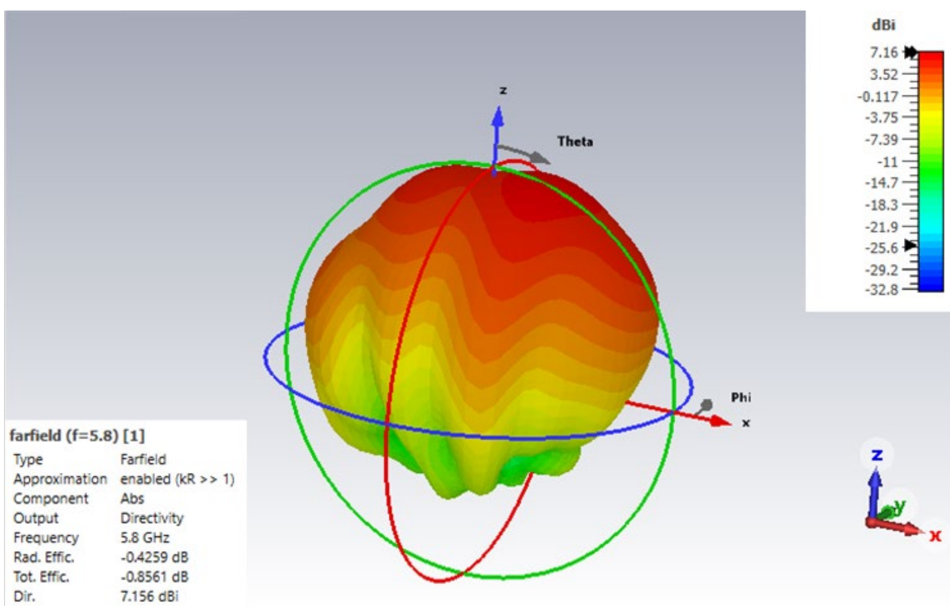

Figure B-6. 3D farfield of 3D-printed antenna: element 1.

Appendix C. Antenna Characterization Code

```
# Antenna Characterization
import gpib*
import time
import numpy as np
import os

################# Functions ##################################
# write cmd and read float
# use for reading CP, WL, and CL
def rd_f_gpib(inst,cmd):
    if not debug:
        inst.write(cmd)
        tmp = inst.read(100)
        tmp = tmp.decode('utf-8')
        #change byte string to normal string, doesn't seem to return fractional numbers
        return float(tmp[0:4])
    else:
        return 0

# write cmd and read float
# use for reading NA, format is long
def rd_flong_gpib(inst,cmd):
    if not debug:
        inst.write(cmd)
        tmp = inst.read(100)
        tmp = tmp.decode('utf-8')
        #change byte string to normal string, doesn't seem to return fractional numbers
```

* GPIB drivers were obtained from https://gist.github.com/ochococo#linux-gpib

```
            return float(tmp[0:19])
        else:
            return 0

# query inst and return string
def rd_s_gpib(inst,s):
        if not debug:
            inst.write(s)
            r = inst.read(100)
            return r
        else:
            return "debug"

# write string
def wr_s_gpib(inst,s):
        if not debug:
            inst.write(s)

# goto target angle v
def goto_tg(inst,v):
        if not debug:
            cmd="TG "+ str(v)
            inst.write(cmd)
            #print(cmd)
            inst.write("SK")
            cp = rd_f_gpib(inst,"CP?")
            while cp != v:
                cp = rd_f_gpib(inst,"CP?")
                #print(cp,", goal = ",v)
                time.sleep(debug_delay)
```

```
        return cp
    else:
        time.sleep(0.5)
        return v

################ parameters ###################################
# Az looking at positioner from tx ant, pos is to left, neg is to right
# Az = 0 points round to tx ant, Az = 90 faces round perpendicular to tx ant

# El 90 is ant array facing down, 180 faces tx antenna
# looking into end of round, pos is CCW, neg is CW
# pos turns up, neg turns down (if az zero is 90)

# will go from zero-fov/2 to zero+fov/2, in steps of res
# if do el sweep, make az FOV = 0, and vice versa
az_zero = 90
az_fov = 0
az_res = 10
el_zero = 180
el_fov = 180
el_res = 10

basename = "data_na_el_res10_ant1_5p8"
print("basename = ",basename)
debug = False
debug_delay = 0.1
DSIZE=1

################# Init ########################################
time1=time.time()
```

```
### GPIB setup
if not debug:
    instAz = Gpib.Gpib(0,9) # first is usually 0, then GPIB address
    instEl = Gpib.Gpib(0,8)
    instNA = Gpib.Gpib(0,17)
else:
    instAz = 0
    instEl = 0
# Check comms
print("Az inst is ",rd_s_gpib(instAz,"*IDN?")) #this is byte string, not normal string
print("El inst is ",rd_s_gpib(instEl,"*IDN?")) #this is byte string, not normal string
print("NA inst is ",rd_s_gpib(instNA,"*IDN?")) #this is byte string, not normal string
# Set Az limits
# 90 is zero, so 0 to 180 should be limits for +-90 sweep
wr_s_gpib(instAz,"WL 180")
wr_s_gpib(instAz,"CL 0")
# Set El limits
# 180 is zero, so 90 to 270 should be limits for +-90 sweep
wr_s_gpib(instEl,"WL 270")
wr_s_gpib(instEl,"CL 90")
# Check CP and limits
print("AZ cp =",rd_f_gpib(instAz,"CP?"),", cw limit =",
rd_f_gpib(instAz,"WL?"),", ccw limit =",rd_f_gpib(instAz,"CL?"))
print("EL cp =",rd_f_gpib(instEl,"CP?"),", cw limit =",
rd_f_gpib(instEl,"WL?"),", ccw limit =",rd_f_gpib(instEl,"CL?"))


################ data setup ####################
```

```
# some setup
azn=int((az_fov/az_res)+1)
eln=int((el_fov/el_res)+1)
datan=azn*eln
print("datan = ",datan, ", eln = ", eln, ", azn = ", azn)

############## main loop ###########################################
az=az_zero - az_fov/2 # az start
el=el_zero - el_fov/2
angle = goto_tg(instAz,az)
print("goto az ",angle)
time.sleep(2)

print("\nStarting at az = ", az, ", el = ",el)
el_dir = 1
n = datan
data=np.zeros([azn,eln],dtype=np.float64)

for azi in range(azn):
        angle = goto_tg(instAz,az)
        print("goto az ",angle)
        time.sleep(1)

        for eli in range(eln):
                angle = goto_tg(instEl,el)
                print("goto el ",angle)
                time.sleep(1)
                print("************** az,el = ",az,",",el)

                tmp = rd_flong_gpib(instNA,"CALC1:MARK1:Y?")
```

```
                time.sleep(1)
                print(tmp)
                data[azi,eli] = tmp
                if eli < eln-1:
                    el=el+(el_res*el_dir) #don't inc if last one
        el_dir=el_dir*-1
        az=az+az_res

print("done!!!!!!!!! ",time.time()-time1)

#if done, save data
filename = basename + ".dat"
data.tofile(filename)
print("saving ",filename)
os.chmod(filename,0o777)
```

List of Symbols, Abbreviations, and Acronyms

3D	three-dimensional
ARL	Army Research Laboratory
AUT	antenna under test
COTS	commercial off-the-shelf
DEVCOM	U.S. Army Combat Capabilities Development Command
DOA	direction of arrival
GPIB	general purpose interface bus
ISM	industrial, scientific, and medical
M&S	modeling and simulation
SLS	selective laser sintering
USB	Universal Serial Bus

1 DEFENSE TECHNICAL
(PDF) INFORMATION CTR
DTIC OCA

1 DEVCOM ARL
(PDF) FCDD RLB CI
TECH LIB